Theoretical and Applied Climatology (2019) 136:15–30
https://doi.org/10.1007/s00704-018-2460-2

ORIGINAL PAPER

Rainfall erosivity and sediment load over the Poyang Lake Basin under variable climate and human activities since the 1960s

Chaojun Gu[1] · Xingmin Mu[1,2] · Peng Gao[1,2] · Guangju Zhao[1,2] · Wenyi Sun[1,2] · Qiang Yu[1]

Received: 24 March 2017 / Accepted: 12 March 2018 / Published online: 26 March 2018

Abstract

Accelerated soil erosion exerts adverse effects on water and soil resources. Rainfall erosivity reflects soil erosion potential driven by rainfall, which is essential for soil erosive risk assessment. This study investigated the spatiotemporal variation of rainfall erosivity and its impacts on sediment load over the largest freshwater lake basin of China (the Poyang Lake Basin, abbreviate to PYLB). The spatiotemporal variations of rainfall erosivity from 1961 to 2014 based on 57 meteorological stations were detected using the Mann–Kendall test, linear regression, and kriging interpolation method. The sequential *t* test analysis of regime shift (STARS) was employed to identify the abrupt changes of sediment load, and the modified double mass curve was used to assess the impacts of rainfall erosivity variability on sediment load. It was found that there was significant increase ($P < 0.05$) in rainfall erosivity in winter due to the significant increase in January over the last 54 years, whereas no trend in year and other seasons. Annual sediment load into the Poyang Lake (PYL) decreased significantly ($P < 0.01$) between 1961 and 2014, and the change-points were identified in both 1985 and 2003. It was found that take annual rainfall erosivity as the explanatory variables of the double mass curves is more reasonable than annual rainfall and erosive rainfall. The estimation via the modified double mass curve demonstrated that compared with the period before change-point (1961–1984), the changes of rainfall erosivity increased 8.0 and 2.1% of sediment load during 1985–2002 and 2003–2014, respectively. Human activities decreased 50.2 and 69.7% of sediment load during the last two periods, which indicated effects of human activities on sediment load change was much larger than that of rainfall erosivity variability in the PYLB.

1 Introduction

Soil loss and soil degenerated by erosion are one of the most serious environmental problems in the world (Renschler et al. 1999; Meusburger et al. 2012). It was reported that approximately 1047 million ha (Mha) of global land area was affected by erosion, of which 751 Mha was severely affected by water erosion, and 296 Mha by wind erosion in the late 2000s (Scherr and Yadav 1996; Lal 2003). Soil erosion accelerates river channel sedimentation, aggravates geological disasters (e.g., landslide, collapse, and debris flow), destroys the shipping, and all of them significantly affect the development of economy and society for a country (Bonilla and Vidal 2011; Lai et al. 2016). Quantitative evaluation of the soil erosion risk is of considerable interest to agricultural protection, soil conservation, disaster control, water resources, and hydraulic structure management (Lai et al. 2016). Water erosion being the most widely distributed erosion type across the world, which has been extensively assessed previously based on various soil erosion and sediment transport models, such as universal soil loss equation (USLE) (Wischmeier and Smith 1958), revised universal soil loss equation (RUSLE) (Renard et al. 1997), Water Erosion Prediction Project (WEPP) (Flanagan and Nearing 1995), and European Soil Erosion Model (EUROSEM) (Morgan et al. 1998).

The rainfall erosivity, R, which combines the effects of duration, magnitude, and intensity of rainfall events, is essential

✉ Peng Gao
gaopeng@ms.iswc.ac.cn

[1] State Key Laboratory of Soil Erosion and Dryland Farming on the Loess Plateau, Northwest A&F University, Xinong Road 26, Yangling 712100, Shaanxi Province, China

[2] Institute of Soil and Water Conservation Chinese Academy of Sciences and Ministry of Water Resources, Northwest A&F University, Xinong Road 26, Yangling 712100, Shaanxi Province, China

for a series of soil erosion models (e.g., USLE, RUSLE) (Lai et al. 2016). Rainfall erosivity is not amenable to human modification that is different from soil characteristics, vegetation cover, and soil conservation (Angulo-Martínez and Beguería 2009). It represents the potential ability of rainfall to cause erosion, thus it reflects the soil erosion risk when the underlying surface condition is invariable for a region. In the classic USLE and RUSLE models, R of a given storm was initially defined as the rainfall energy multiplied by the maximum 30-min rainfall intensity, i.e., EI30, and the annual R was the sum of EI30 calculated from a rainfall record (Wischmeier and Smith 1978). Since it has been put forward, the expression was widely used and tested throughout the world (Van der Knijff et al. 2000; Shi et al. 2004; Onori et al. 2006; Romero et al. 2007). However, the main disadvantage of USLE (RUSLE) R factor is that it needs a continuous rainfall data (at least 15 min). Such a high time resolution data are not available for many countries and regions, and to process these data is highly tedious and time-consuming (Angulo-Martínez and Beguería 2009; Huang et al. 2013; Lai et al. 2016). As a consequence, numerous studies have established a statistical regression equation between R and precipitation variables, such as annual precipitation (Renard and Freimund 1994), monthly precipitation (Oduro-Afriyie 1996), and daily precipitation (Yu and Rosewell 1996; Zhang et al. 2002). These simplified methods offer great convenience to investigate the spatial and temporal variation of the rainfall erosivity.

China is one of the countries that suffer from most serious soil erosion in the world. The water erosion area covers about 164.88×10^4 km^2, which account for 17.53% of the national area (Xiaoli et al. 2002). Under the global warming background, extreme rainfall events in China were increased and intensified (Xu et al. 2009; Sun et al. 2016), which might affect the characteristics of water erosion in different time and region. Hence, it is in great need to investigate the spatial temporal variation of rainfall erosivity. However, the studies of rainfall erosivity were difficult and non-systematized previously owning to the limitations of the computing method. In 2002, Zhang et al. (2002) proposed a new and simple method to calculate R based on daily rainfall data, which brought about great progress in the study of rainfall erosivity in China. After that, numerous documents of rainfall erosivity in various regions were reported (Xin et al. 2011; Huang et al. 2013; Lai et al. 2016), but few studies concerned the PYLB. The PYL, being the biggest freshwater lake in China, plays a vital role in social and economic development in the surrounding area (Zhang et al. 2011a, b). Moreover, the PYL is naturally connected with the middle reach of the Yangtze River, whose capacity is important in the mitigation and control of flood hazards of the Yangtze River (Zhang et al. 2011a, b). Therefore, serious soil erosion in the PYLB is negative to the protection of the Poyang Lake ecosystem. Remote sensing investigation showed that erosion areas in the PYLB reached approximately 35,221 km^2 in 1996, accounting for 21.71% of the PYLB, of which more than 90% was formed by water erosion (Shi et al. 2008). Moreover, frequencies of extreme precipitation, such as max 1-day precipitation amount (RX1day) and max 5-day precipitation amount (RX5day), increased significantly in winter and summer months (Zhang et al. 2016b). Under such a climatic background, it is meaningful for basin-scale conservation of the aquatic ecosystems to thorough investigates the change characteristics of the rainfall erosivity.

Changes in rainfall erosivity will significantly influence the sediment yield at different spatial and temporal scales. On the other hand, sediment yield is affected by human activities, such as deforestation, land clearance, mining, and construction of reservoirs (Walling 2006). The dynamics of sediment yield is more complex than rainfall erosivity. Zhang et al. (2011a, b)) examined the temporal trends of sediment load from 1955 to 2005 in five tributaries of the PYLB using Mann–Kendall trend test. The results showed that sediment load of mostly tributaries increased before the 1980s, while decreased significantly thereafter. Similar results were found that sediment load inputs of the PYL were significantly decreased during 1956–2008 (Luo et al. 2015). However, to what extent are climate change and human activities responsible for the decline of the sediment load? The above documents did not answer. Furthermore, the relationship between rainfall erosivity and sediment load in the PYLB was rarely reported in the last half century. Therefore, the objects of this study are (1) to statistically analyze the spatiotemporal variation of rainfall erosivity in the PYLB; (2) to examine the trends and shifts of sediment load inputs of the PYL; (3) to identify the relationship between rainfall erosivity and sediment load; and (4) to assess the effects of rainfall erosivity variability on sediment load inputs of the PYL.

2 Study area and dataset

2.1 The study area

The PYL (28° 22′–29° 45′ N, 115° 47′–116° 45′ E) is located in the southern middle reaches of the Yangtze River (Fig. 1a). The lake water level fluctuates greatly due to the uneven distribution of rainfall during a year. The lake area can reach up to 4000 km^2 in summer (June–September) while shrinks to less than 3000 km^2 in autumn (October–November) and winter (December–February) (Gu et al. 2016a, b). The total drainage area of the water systems of the PYLB is 162,200 km^2, accounting for 9% of the drainage area of the Yangtze River Basin (Zhang et al. 2011a, b). There are mainly five large

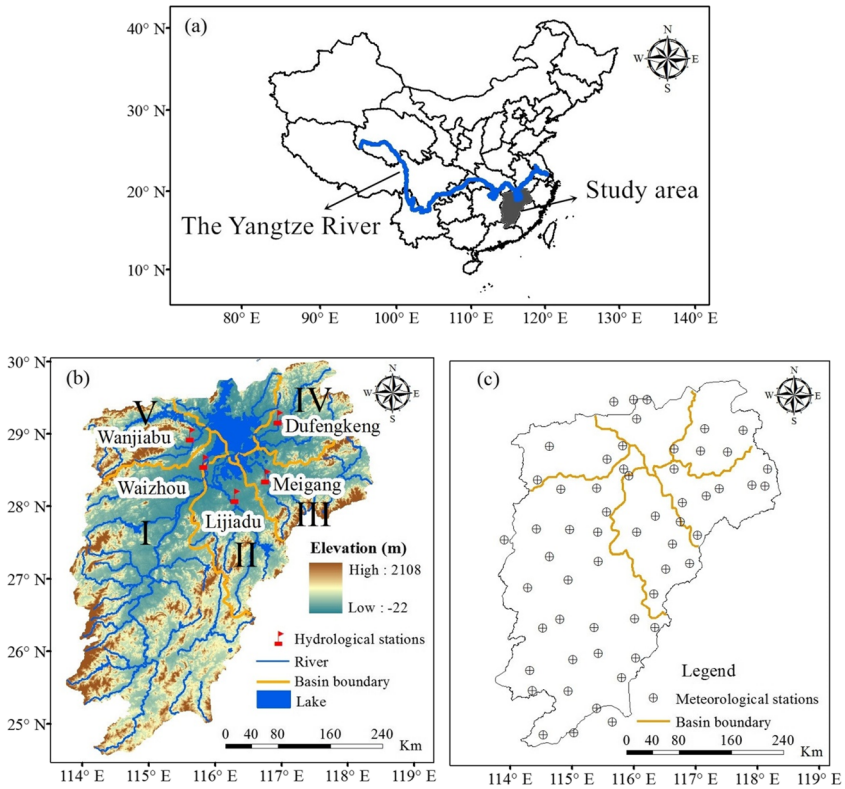

Fig. 1 The location of the Poyang Lake basin (**a**). Location of the five main tributaries and the five hydrological stations in the Poyang Lake basin (**b**). Distribution of the 57 meteorological stations (**c**)

tributaries within the PYLB, namely, Ganjiang River (I), Fuhe River (II), Xinjiang River (III), Raohe River (IV), and Xiuhe River (V) (Fig. 1b). The topography in the PYLB is diverse, including mountains, hills, and alluvial plains. Mountains spread mainly in the western and eastern parts, with a maximum elevation of 2108 m above the sea level, while low alluvial plains are primarily in its central areas. Because the lake has high biodiversity, flood storage function, and natural resources, thus considerable importance has been attached to the lake by local and central governments of China (Zhang et al. 2016a). In 2009, the Chinese State Council approved "Poyang Lake Ecological Economic Zone Planning" (Zhang et al. 2016a, b). It is an important opportunity to develop the economy of the PYLB, which is also a challenge for the environment in the PYLB.

2.2 Data

Daily rainfall data between 1961 and 2014 obtained from 57 meteorological stations were used for rainfall erosivity calculation (Fig. 1c). The data were collected from the National Climatic Centre of the China Meteorological Administration (CMA). The areal mean rainfall and rainfall erosivity was derived from arithmetic mean. Annual sediment load data were collected from five hydrological stations of the five main tributaries in the PYLB. Among these stations, Waizhou, Lijiadu, and Meigang stations are located at the outlet of the Ganjiang River, Fuhe River, and Xinjiang River; Dufengkeng and Wanjiabu stations are located at the branches of the Raohe River and Xiushui River (Fig. 1b). The total sediment load into the PYL was the sum of the observed values at the five stations. The consistency, continuity, and quality of the data were verified by the corresponding institutions before their releases.

3 Methodologies

3.1 Rainfall erosivity model

Long-term (> 30 years) and high temporal resolution (at least 15 min) record of rainfall is not available for the meteorological stations in China. We applied Zhang's model to calculate rainfall erosivity (Zhang et al. 2002). This model has been widely used in China and was tested in many regions of China (Ma et al. 2009; Xin et al. 2011; Huang et al. 2013). The key point of this model is to determine erosive rainfall standard. It usually uses 12 mm day^{-1} as a mean value of the erosive rainfall in China, while this standard may cause uncertainties in different areas. Qin et al. (2013) defined erosive rainfall standards as 10.0 mm day^{-1} in northern PYLB based on field observation data from runoff plots. Thus, we employed 10.0 mm day^{-1} as the erosive rainfall standard to calculate the rainfall erosivity in this study.

The method drives annual, seasonal, and monthly rainfall erosivity through accumulating value of half-month rainfall erosivity. The half-month rainfall erosivity (M_i) (MJ mm ha^{-1} h^{-1}) was calculated using Eq. (1).

$$M_i = a\sum_{j=1}^{k}(D_j)^b \tag{1}$$

where D_j is the effective rainfall for day j in one half-month, and it is equal to the actual rainfall if the actual rainfall is higher than the threshold value of 10 mm day^{-1}; otherwise, Dj is equal to zero. The term k is the number of days in the half month. The terms a, b are the parameters. Parameter b was estimated by erosive rainfall, which was given as Eq. (2) according to Zhang et al. (2002).

$$b = 0.8363 + \frac{18.177}{\overline{P}_{d10}} + \frac{24.455}{\overline{P}_{y10}} \tag{2}$$

where $\overline{P}_{d10}$ is the average daily rainfall that is higher than 10 mm, and $\overline{P}_{y10}$ is the yearly average rainfall for days with rainfall higher than 10 mm day^{-1}.

Parameter a was determined based on parameter b and was calculated as follows (Zhang et al. 2002; Xin et al. 2011; Huang et al. 2013):

$$a = 21.486b^{-7.1891} \tag{3}$$

3.2 Trend test

The Mann–Kendall (MK) statistical test was used for trend detection. The MK test is a non-parametric method, which is robust to non-normally distributed and censored data in hydro-climatic time series (Mann 1945; Kendall 1975). However, the efficiency of the MK test will be reduced by the serial correlation of the time series (Von Storch 1999). Serial correlation should be removed before conducting the MK trend test. The trend-free prewhitening (TFPW) method (Yue and Wang 2004) was applied to remove any significant linear trend from the raw time series and serial correlation. A statistic (Z) was obtained from the MK test on the whitened series from TFPW method. A negative value of Z indicates a downward trend, and vice versa. $|Z| \geq 1.96$ (2.56) means the trend is significant at 0.05 (0.01) significance levels (α).

The change rate of hydro-climatic series is given by the linear tendency estimation method (Sun et al. 2013). The linear tendency estimation method can be expressed as follows:

$$x_t' = \beta t + c \tag{4}$$

where x_t' represents the fitted value of the variable, β indicates the change rate, t means the time, and c is the intercept.

3.3 Spatial interpolation method

In order to investigate the spatial distribution of rainfall erosivity across the PYLB, the mean values and change rate (β) of rainfall erosivity were interpolated by kriging interpolation technology with ArcGIS 9.3 software package (Lai et al. 2016).

3.4 Change-point analysis

The sequential t test analysis of regime shift (STARS) was employed to examine the abrupt changes of the sediment load time series. The STARS was proposed by Rodionov (Rodionov 2006), which can be used to detect multiple change points of a hydro-climatic time series (Zhao et al. 2017). For a time series, the mean value of the first regime (R1) is estimated as

$$\overline{x}_{R1} = \frac{1}{m}\sum_{k=1}^{m} x_k \qquad 1 \leq k \leq m \tag{5}$$

where m is the cutoff length of the regimes to be tested. The difference between the mean value of a new regime (R2) and the current regime (R1) can be estimated according to the Student's t test:

$$\varphi = \overline{x}_{R2} - \overline{x}_{R1} = t\sqrt{2\sigma_m^2/m} \tag{6}$$

where t is the value of the t-distribution with $2m$ - 2 degrees of freedom at a probability level P. σm is the average standard deviation for m-year intervals in the time series. A test is performed between the mean values of the subseries x_1, x_2, …, x_m and x_{m+1} to determine statistically significant deviations. A year with a significant deviation is marked as a potential change point j, and subsequent observations are used to confirm or reject the hypothesis. The regime shift index (RSI) is estimated to confirm or reject the null hypothesis of the regime shift starting in year j:

$$RSI_{i,j} = \sum_{i=j}^{j+q} \frac{x_i - \left(\overline{x}_{R1} + \varphi\right)}{m\sigma_m} \qquad q = 0, 1, \cdots, m-1 \tag{7}$$

If the RSI retains the same sign as that in year j, then it would increase the confidence that a shift did occur. Otherwise, the start point j is false. Once a new regime is determined, it is considered the base regime. Regime shift is searched continuously until all the available data were evaluated.

3.5 Wavelet analysis

Wavelet analysis can reflect the localized variation in both time and frequency of time series (Torrence and Compo

1998). We used wavelet transform method to investigate the periodicity of sediment load and rainfall erosivity. The key for the wavelet analysis is the choice of wavelet function. The Morlet wavelet function has a phase difference of π/2 in the real part and imaginary part, which can eliminate false oscillations (He et al. 2013). Hence, results of Morlet wavelet analysis are more accurate. The complex Morlet wavelet φ(t) and wavelet variance Var(a) were defined as follows:

$$\varphi(t) = e^{ict}e^{-t^2/2} \tag{8}$$

$$\mathrm{Var}(a) = \sum(\mathrm{W_f})^2(a,b) \tag{9}$$

where c is a constant and i denotes the imaginary part. $W_f(a,b)$ is the wavelet coefficient, a is the frequency/scale variable, and b is the time variable. $W_f(a,b)$ reflects the oscillation characteristics of the time series. Peak value of Var(a) indicates the main period of the time series. The maximum value at the peak was the first main period, which is used to analyze periodic oscillation of time series. The second and third peak value of Var(a) corresponding to the second and third main periods.

3.6 Double mass curve

Double mass curve was used to detect inconsistencies in two hydrological elements which result from human activities. For two variables such as x and y, they all have n-year observations. Then, their cumulative values (X_i and X_i, $i = 1, 2, 3, \ldots, n$) can be expressed as follows:

$$X_i = \sum_1^i x_i \tag{10}$$

$$Y_i = \sum_1^i y_i \tag{11}$$

As shown in the Fig. 2, draw X_i and Y_i in the same coordinate system, and the plot follows a straight line if the proportionality between the two variables remain unchanged (OAA′). The slope of the line represents the constant of proportionality between the quantities (k_1). A change in the slope of the curve may deduce that the characteristics of the quantities have changed. It means y_i increased after an abrupt year if the slope after the change-point year is higher than before the change-point (AB). Otherwise, y_i is decreased after an abrupt year (AC).

To estimate the impacts of X change on Y, linear regression equations without intercept can be established according to the double mass curves before the change-point (OA). We could extend the linear equations to the periods after change-point (AA′) if the fitting efficiency is significant ($P < 0.05$), and the theoretical Y after change-point (Y_P) can be calculated as

$$Y_P = k_1 \times X \tag{12}$$

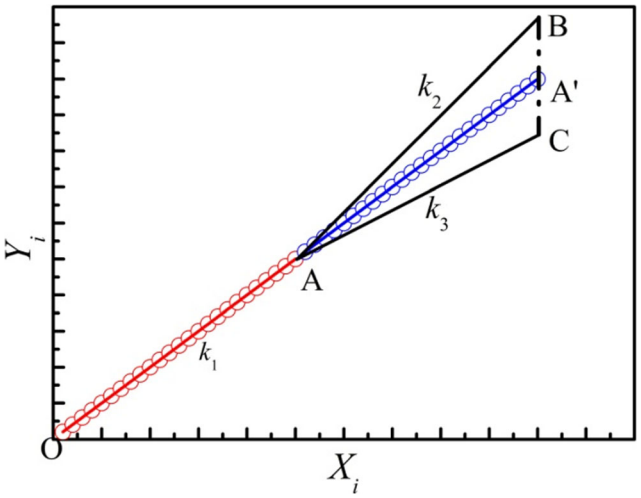

Fig. 2 Sketch map of double mass curve

The impacts of X change on Y (ΔY_X) can be estimated as

$$\Delta Y_X = k_1 \times \Delta X \tag{13}$$

ΔX is the difference of X between the periods before change-point and the periods after change-point. Positive (negative) ΔX means X change increased (decreased) Y. Then, the effects of X change on Y (I_x) can be calculated as follows:

$$I_x = \frac{\Delta Y_X}{Y_P} \times 100\% \tag{14}$$

Thus, the impacts of other factors on Y (I_h, i.e., A′B or A′C in Fig. 2) express as

$$I_h = \frac{Y_P - Y_o - \Delta Y_X}{Y_P} \times 100\% \tag{15}$$

where Y_o is the practical Y after the change-point. Traditionally, X indicates annual rainfall, and Y indicates the annual sediment load or annual runoff.

4 Results

4.1 Spatiotemporal variation of rainfall erosivity

Annual average of rainfall, erosive rainfall, and rainfall erosivity of the PYLB from 1961 to 2014 are 1633.5 mm year^{-1}, 1328.6 mm year^{-1}, and 9905.0 MJ mm ha^{-1} h^{-1} year^{-1}, respectively. The coefficient of variation (CV) of rainfall erosivity was the maximal among the variables, showing the highest variability. Smoothed trend indicated that rainfall and rainfall erosivity showed distinct interannual and decadal variations (Fig. 3a). Average annual values of the three variables in the 1990s were the highest among decades, immediately followed by a low period in the 2000s. The change rates for annual rainfall, erosive rainfall, and rainfall erosivity were 1.8 mm year^{-1},

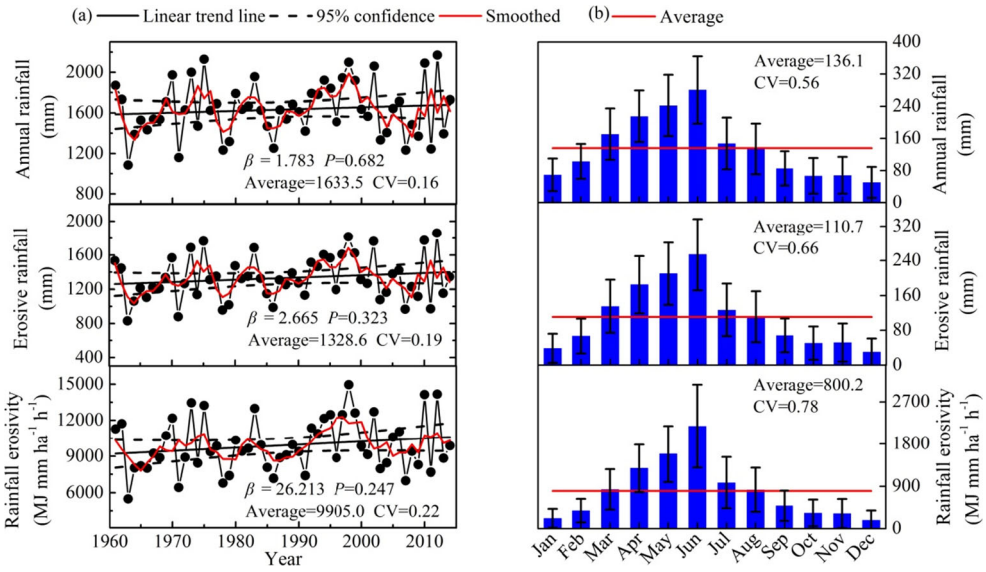

Fig. 3 The inter-annual (**a**) and intra-annual (**b**) variation of annual rainfall, erosive rainfall, and rainfall erosivity over the PYLB

2.7 mm year^{-1}, and 26.2 MJ mm ha^{-1} h^{-1} year^{-1}. Intra-annual variations of rainfall and rainfall erosivity were asymmetrical (Fig. 3b). Rainfall and rainfall erosivity increased from January to June, peaking in June, and then abruptly decreased. The rainy season across the Poyang Lake basin starts in April and ends in July, which accounts for more than 54.2% of the annual rainfall. Intra-annual fluctuation of erosive rainfall and rainfall erosivity are higher than annual rainfall, especially for rainfall erosivity (CV = 0.78). The rainfall erosivity between April and July accounts for 62.8% of the annual rainfall erosivity.

Spatial distributions of annual rainfall, erosive rainfall, and rainfall erosivity showed synchronized variation (Fig. 4a–c). Rainfall erosivity showed a northeast increasing trend as annual rainfall (Fig. 4c). Average annual rainfall erosivity was

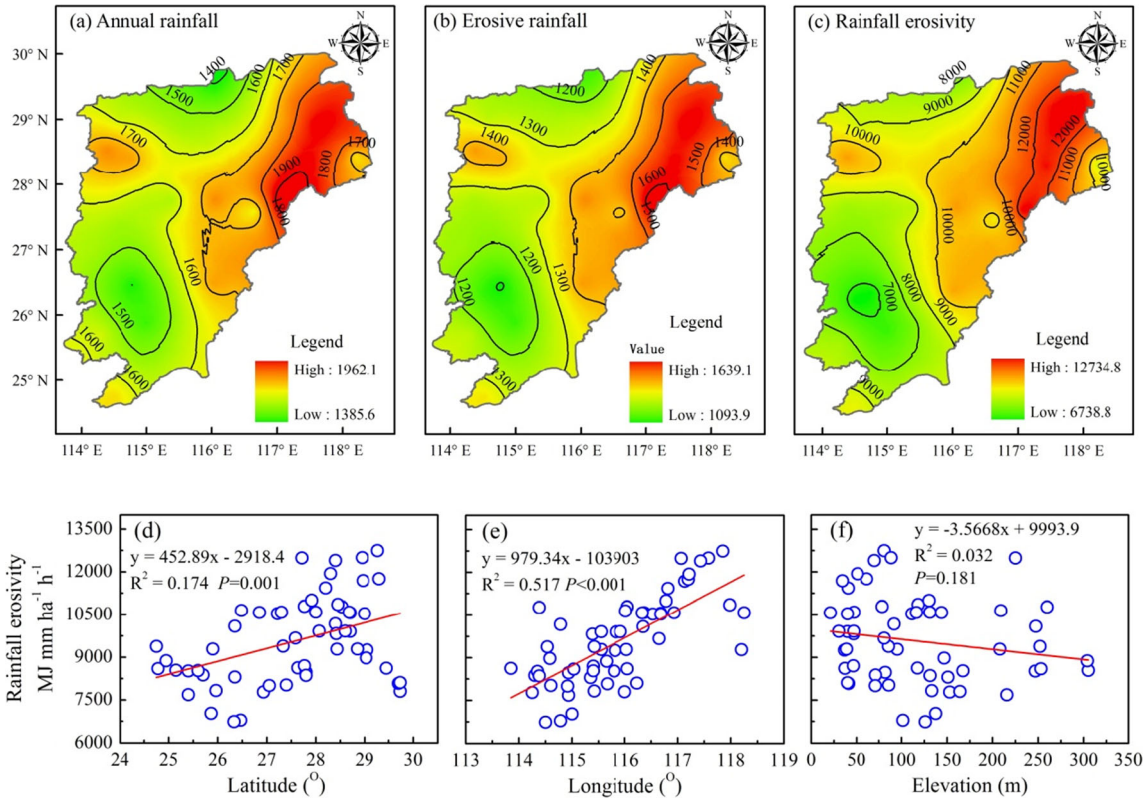

Fig. 4 Spatial distributions of annual rainfall (**a**), erosive rainfall (**b**), rainfall erosivity (**c**), and the relationships of rainfall erosivity with latitude (**d**), longitude (**e**), and elevation (**f**) in the PYLB

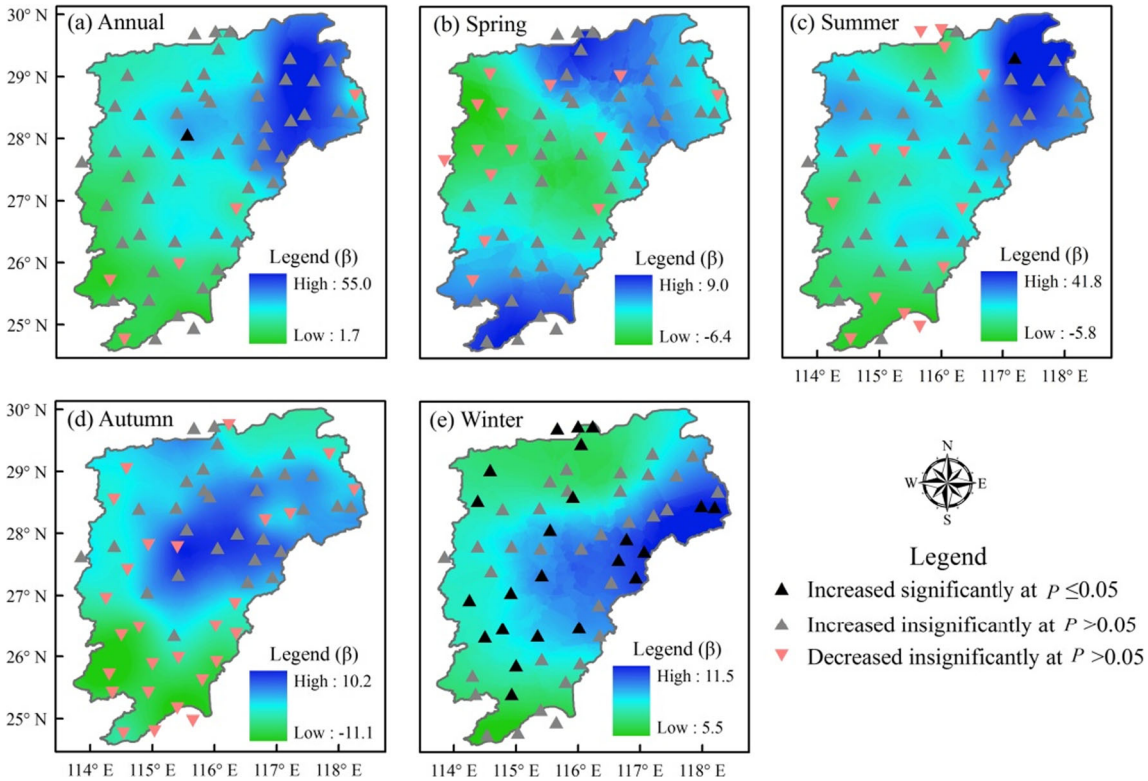

Fig. 5 Spatial distributions for trends of annual (**a**) and seasonal (**b**–**e**) rainfall erosivity during 1961–2014 in the PYLB (spring: March–May; summer: June–August; autumn: September–November; winter: December–February)

less than 8000 MJ mm ha^{-1} h^{-1} $year^{-1}$ in southwest of the PYLB, while it is larger than 10,000 MJ mm ha^{-1} h^{-1} $year^{-1}$ in the eastern region. Moreover, rainfall erosivity has the best correlation with longitude ($r = 0.719$, $P < 0.001$) (Fig. 4d–f), indicating longitude was the main axis of spatial variation of rainfall erosivity in the PYLB.

Figure 5a indicates that annual rainfall erosivity over the PYLB increased in the last 54 years, and one station was in significant increasing trend. The annual change rate ranged from 1.7 to 55.0 MJ mm ha^{-1} h^{-1} $year^{-1}$, and the relative higher values was mostly in northeast areas. Seasonally, winter had the most stations (40.3%) with significant increasing trends at 0.05 significance levels, and the ascent rate increased from western to eastern (Fig. 5b–e). For monthly rainfall erosivity, January had the most stations (57.9%) with significant increasing trend, followed by August (15.8%) (Table 1). The significant decreasing trend was only found at two stations in October (Table 1). For April, May, June, September, and December, no significant temporal trend was detected (Table 1).

At basin scales, significant increasing trend was found in January and August (Table 2). Rainfall erosivity of the entire PYLB and the five sub-basins increased significantly in January. In August, most basins showed significant increasing trends except for Ganjiang and Xiuhe basin. At seasonal scales, significant increasing trend of rainfall erosivity was found in winter which could be attributed to the increasing trend in January. At the annual scale, rainfall erosivity for each basin showed no significant temporal trend.

Table 1 Statistics of the 57 meteorological stations' variation trends of monthly rainfall erosivity in the PYLB

Trend	Jan	Feb	Mar	Apr	May	Jun	Jul	Aug	Sep	Oct	Nov	Dec
*	33	1	4	0	0	0	1	9	0	0	1	0
**	23	53	50	20	22	28	47	40	18	16	54	55
***	1	3	3	37	35	29	9	8	39	39	2	2
****	0	0	0	0	0	0	0	0	0	2	0	0

*Significantly increased at $P \leq 0.05$; **increased but not significant at $P \leq 0.05$; ***decreased but not significant at $P \leq 0.05$; ****significantly decreased at $P \leq 0.05$

Table 2 The MK test (Z) and the change rate (β) for rainfall erosivity at basin scale from 1961 to 2014

	The entire PYLB		Ganjiang basin		Fuhe basin		Xinjiang basin		Raohe basin		Xiuhe basin	
	Z	β	Z	β	Z	β	Z	β	Z	β	Z	β
Jan	2.39*	3.37	2.18*	2.77	2.20*	3.89	2.22*	4.19	2.10*	5.47	2.50*	3.64
Feb	1.54	2.55	1.74	2.77	1.35	3.00	1.04	3.23	0.48	0.70	0.75	1.12
Mar	1.13	4.89	1.20	3.56	0.95	5.38	2.01*	9.24	0.92	8.49	0.79	4.08
Apr	0.13	− 0.56	0.04	− 1.38	− 0.42	− 1.30	0.12	0.04	0.34	3.64	0.06	1.97
May	− 0.45	− 3.10	− 0.12	− 0.22	− 0.47	− 8.34	− 0.15	− 6.89	− 0.41	− 8.01	− 0.54	− 6.72
Jun	0.32	1.97	− 0.01	− 3.05	− 0.40	− 1.07	0.35	13.59	0.29	13.04	0.57	6.89
Jul	1.20	5.77	1.79	6.90	1.03	5.54	− 0.09	0.40	0.15	7.40	0.67	4.34
Aug	2.09*	7.04	1.60	4.70	2.52*	8.83	2.17*	8.93	1.96*	18.77	1.51	5.18
Sep	− 0.07	− 1.77	0.31	− 1.79	0.26	− 0.46	− 1.29	− 3.41	0.16	− 0.95	− 0.60	− 3.10
Oct	− 1.61	− 2.67	− 2.02*	− 3.47	− 0.89	− 1.04	− 1.46	− 2.31	0.79	− 1.90	0.04	− 0.83
Nov	1.30	5.25	1.13	4.18	1.13	7.65	1.65	9.45	1.33	6.77	0.98	5.74
Dec	0.97	2.61	0.75	2.44	0.55	3.35	1.53	3.85	1.22	2.90	0.84	1.86
Spring	0.42	1.24	0.56	1.96	− 0.06	− 4.27	0.44	2.40	0.2	4.13	0.10	− 0.68
Summer	1.16	14.77	0.98	8.55	0.72	13.30	0.95	22.92	1.14	39.20	1.24	16.41
Autumn	0.00	0.81	− 0.34	− 1.08	0.75	6.14	0.26	3.73	0.76	3.92	− 0.50	1.81
Winter	2.31*	8.53	2.46*	7.98	2.30*	10.24	2.05*	11.27	1.45	9.07	1.76	6.63
Annual	1.33	25.35	1.22	17.41	0.50	25.42	1.05	40.32	0.92	56.32	1.05	24.16

*Significant at $P \leq 0.05$, others are not significant at $P \leq 0.05$ (spring: March–May; summer: June–August; autumn: September–November; winter: December–February)

4.2 Temporal change in sediment load

The MK test was applied to annual sediment load from 1961 to 2014 (Z value in Fig. 6). There was a significant decreasing trend in total sediment load inputs of the PYL, with a rate of -27.349×10^4 t year^{-1}. For the five tributaries, significant decreasing trend were found in Ganjiang, Xinjiang, and Xiuhe rivers. The descent rates for these river systems were −

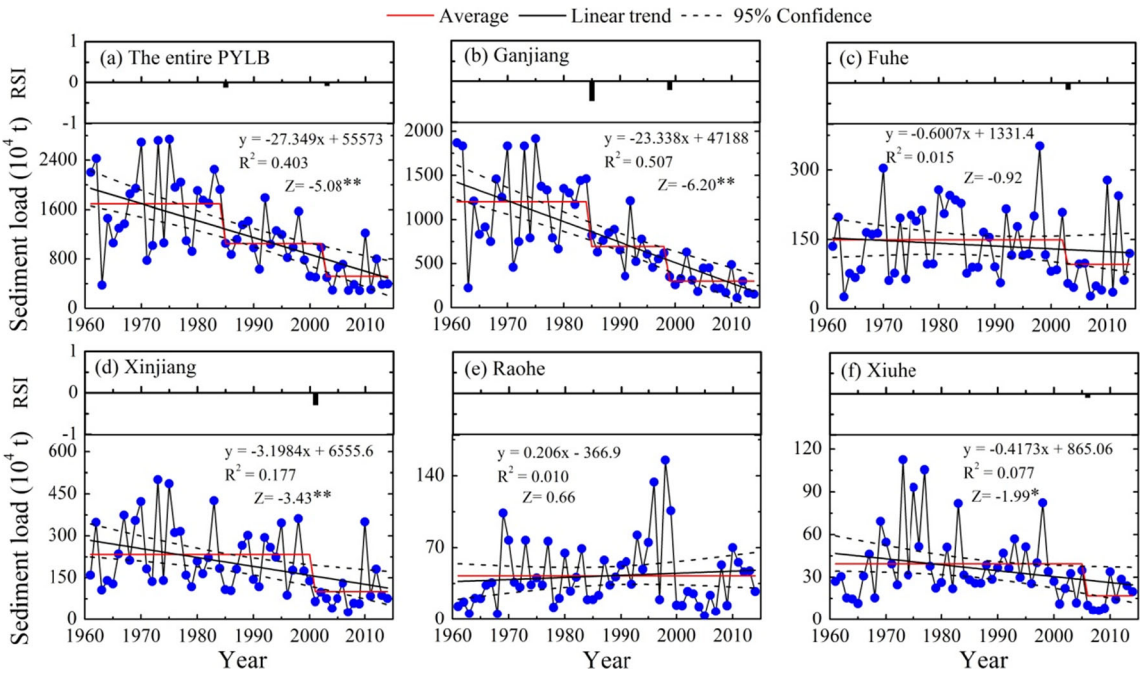

Fig. 6 Change-point analysis of annual sediment load by STARS test over the PYLB from 1961 to 2014 (Z value was the results of MK test, *significant at $P < 0.05$, **significant at $P < 0.01$, others are not significant at $P < 0.05$)

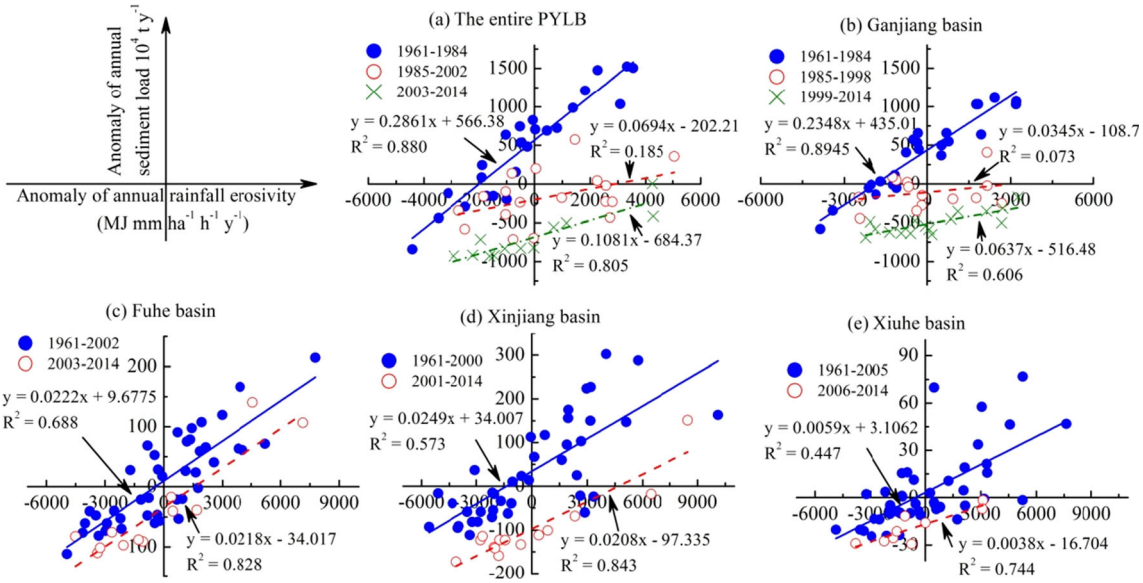

Fig. 7 Relationships between annual sediment load and rainfall erosivity in different periods in the PYLB

23.338×10^4, -3.198×10^4, and -0.417×10^4 t year^{-1}, respectively. No significant temporal trend was found in Fuhe and Raohe rivers. According to the analysis of STARS method, significant downward shifts in annual sediment load of the entire PYLB were found in 1985 and 2003 (Fig. 6a). Similarly, STARS method revealed two change-points for Ganjiang River (1985, 1999) (Fig. 6b), one change-point for Fuhe River (2003) (Fig. 6c), Xinjiang River (2001) (Fig. 6d), and Xiuhe River (2006) (Fig. 6f).

4.3 Correlation and periodic relationship between sediment load and rainfall erosivity

The relationship curves of the anomaly of annual sediment load vs. anomaly of rainfall erosivity are shown in Fig. 7. Majority of points distributed under the x-axis ($y < 0$) after the change-points, which indicated that sediment load were often lower than the long-term average value after the change-points. Chou's F test (Chow 1960) showed that structures of the regression equations between sediment load and rainfall erosivity before and after change-point were significantly different ($P < 0.05$) over the PYLB except for Fuhe River (Table 3). The slopes of the regression equations can be regarded as "sediment generation index," which indicates the sediment generation capacity of unit rainfall erosivity. For the entire PYLB, the index was 0.2861×10^4 t/(MJ mm ha^{-1} h^{-1}) during 1961–1984, while it was only 0.0694×10^4 and 0.1081×10^4 t/(MJ mm ha^{-1} h^{-1}) during 1985–2002 and 2003–2014. For the tributaries, the index after change-points was all lower than that before change-points. The highest decrease was seen in the Gnjiang River, in which the index during 1985–1998 and 1999–2014 was only 14.7 and 27.1% of the value before change-point. Those much lower sediment load per unit rainfall erosivity demonstrated that regional rainfall erosivity variability was insufficient to explain the significant decrease in sediment load.

The wavelet variance showed that annual rainfall erosivity and sediment load across the PYLB generally have the same main period except for Xiuhe basin (Fig. 8a). For the entire PYLB, rainfall erosivity and sediment load possess the main periods of 11, 6 and 18–19, and 11 years corresponding to their first main period (Fig. 8a). The

Table 3 Results of Chou's F test for the regression equations between sediment load and rainfall erosivity before and after change-point

Basin	Period	Period	Basin	Period
The entire PYLB	1985–2002	2003–2014	Xinjiang	2001–2014
	6.81**	16.53**		8.48**
Gnajiang basin	1985–1998	1999–2014	Xiuhe	2006–2014
	5.88**	27.87**		3.64*
Fuhe basin	2003–2014			
	2.08			

*Significant at $P \leq 0.05$; **significant at $P \leq 0.01$, others are not significant at $P \leq 0.05$

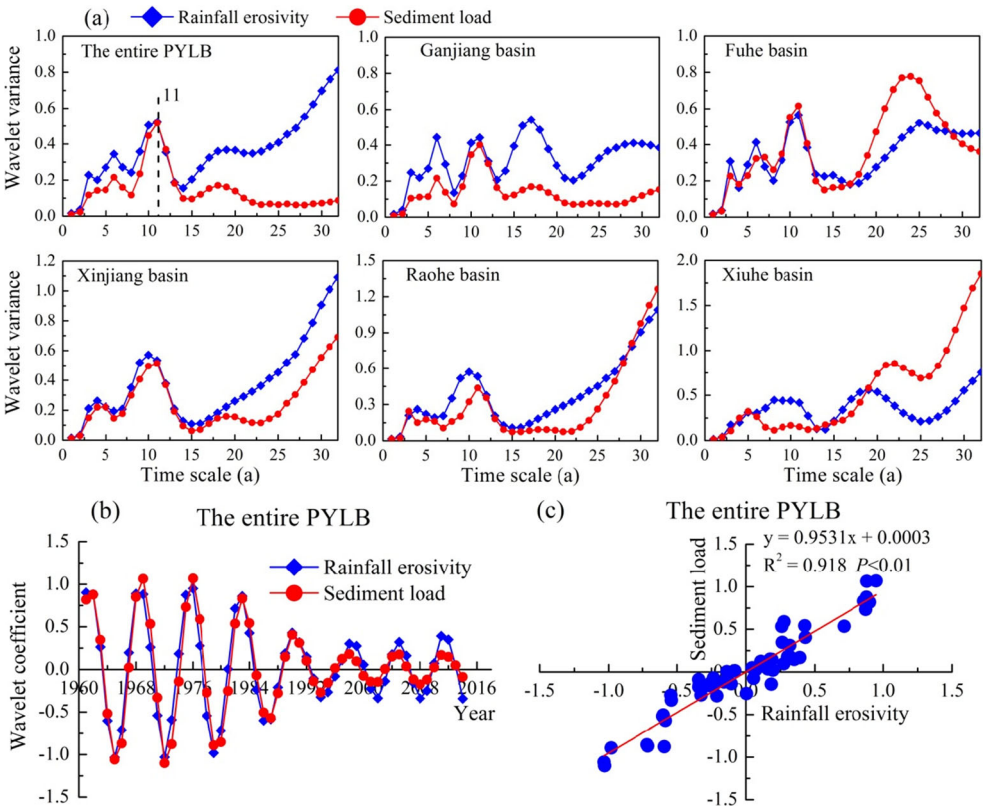

Fig. 8 Wavelet variance of rainfall erosivity and sediment load across the PYLB (**a**), the wavelet coefficient of the first main period (**b**), and their relationships (**c**) of the rainfall erosivity and total sediment load for the entire PYLB

results illustrated that the periodicity of rainfall erosivity and sediment load have not changed in the past half century. The wavelet coefficients of the first main period of the entire PYLB were extracted to reveal the periodic oscillation of sediment load and rainfall erosivity (Fig. 8b). Positive wavelet coefficients donates high sediment load (rainfall erosivity) period and negative wavelet coefficients donates low sediment load (rainfall erosivity) period. Periodic oscillation of sediment load and rainfall erosivity at 11-year scale was highly consistent ($r = 0.958$, $P < 0.01$) (Fig. 8c). There were circa seven cycles of oscillations with a 7-year average period for sediment load and rainfall erosivity during 1961–2014 at their first main period. Beyond the study period, it is expected the period 2015–2017 corresponds to high sediment load (rainfall erosivity) period whereas low sediment load (rainfall erosivity) period over 2018–2020 (Fig. 8b).

4.4 Impacts of rainfall erosivity on sediment load

Changes in sediment load for a given catchment are determined by both climate variability and human activities. However, it is difficult to quantify the individual impacts, as most changes in sediment load are associated with climate change (e.g., rainfall) and human interventions. Double mass curve is a simple, visual, and practical method to quantify the sediment load changes before and after the change-point years. However, the choice of the explanatory variables will affect the efficiency of the method. Based on the change-point analysis, the whole time series of sediment load were divided into two periods. Effects of human activities on sediment load were limited in the period before change-point, and the sediment load was dominated by climate factors in that period. Correlation analysis indicated sediment load has the best correlation with rainfall erosivity before change-point (Table 4);

Table 4 Pearson's correlation coefficients between sediment load and annual rainfall, erosive rainfall, and rainfall erosivity before the change-point year in the PYLB

	The entire PYLB	Ganjiang basin	Fuhe basin	Xinjiang basin	Xiushui basin
Annual rainfall	0.798*	0.813*	0.710*	0.597*	0.600*
Erosive rainfall	0.806*	0.822*	0.719*	0.622*	0.599*
Rainfall erosivity	0.938*	0.946*	0.829*	0.757*	0.668*

*Significant at $P \leq 0.01$

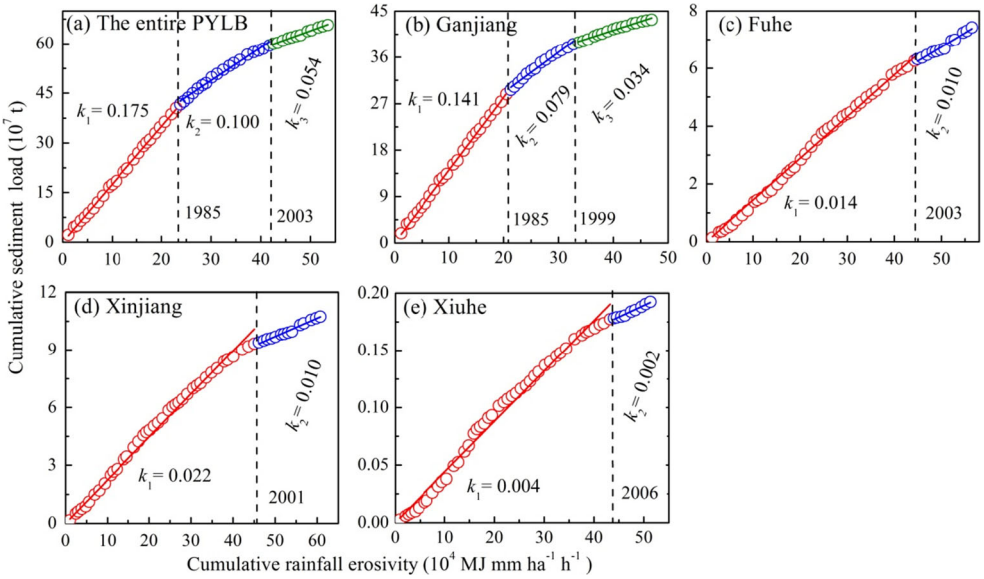

Fig. 9 Double mass curves of rainfall erosivity and sediment load from 1961 to 2014

thus, rainfall erosivity was selected as the explanatory variables of the double mass curves.

Modified double mass curves, along with the linear regression lines of the entire PYLB as well as the four tributaries, are plotted in Fig. 9. The slopes of regression lines after change-point were lower than slopes before change-point for the entire PYLB and the four tributaries, suggesting the change-points identified by STARS method are correct and meaningful. The high fitting efficiency ($P < 0.001$) of the regression equations before change points indicated the linear relation between sediment load and rainfall erosivity was constant (Table 5). Therefore, we could use the double mass curves to estimate the impacts of rainfall erosivity variation on sediment load.

The effects of rainfall erosivity variability and human activities on sediment load in the PYLB are shown in Table 6. The observed sediment load in the PYLB decreased dramatically after the changes-points while the rainfall erosivity varied moderately. Taking the entire PYLB as an example, average annual sediment load during 1985–2002 and 2003–2014 was 636.6×10^4 t year^{-1} (37.7%) and 1158.1×10^4 t year^{-1} (67.1%) lower than the sediment load during 1961–1984 (1690.4×10^4 t year^{-1}). However, average annual rainfall erosivity variability during 1985–2002 and 2003–2014 was 834.3 MJ mm ha^{-1} h^{-1} year^{-1} (8.7%) and 208.7 MJ mm ha^{-1} h^{-1} year^{-1} (2.2%) higher than the rainfall erosivity during 1961–1984. Because the rainfall erosivity after change-points was higher than before change-points, thereby the rainfall erosivity variability increased sediment load. The impacts of rainfall erosivity variability on sediment load were 8.0 and 2.1% during 1985–2002 and 2003–2014, respectivity, compared with the period of 1961–1984. Human activities play the primary role in sediment load decline in the entire PYLB, which decreased 50.2 and 69.7% of the sediment load during 1985–2002 and 2003–2014, respectively. For the four sub-basins, the roles of rainfall erosivity change and human activities on sediment load were different. For the Ganjiang basin, rainfall erosivity variability increased sediment load while human activities decreased the sediment load. For Fuhe basin, Xinjiang basin, and Xiuhe basin, rainfall erosivity change and human activities all decreased the sediment load. However, effects of human activities were always higher than the impacts of the rainfall erosivity variability on sediment load.

Table 5 Regression equations in the double mass curves before the change-point in the PYLB

Basin	Equation	Determination coefficient	*F* test	Significance level
The entire PYLB	SL′ = 0.1751RE′	$R^2 = 0.999$	$F(1,24) = 28{,}168.5$	$P < 0.001$
Ganjiang	SL′ = 0.1409RE′	$R^2 = 0.999$	$F(1,24) = 33{,}024.4$	$P < 0.001$
Fuhe	SL′ = 0.0144RE′	$R^2 = 0.995$	$F(1,42) = 12{,}589.0$	$P < 0.001$
Xinjiang	SL′ = 0.0224RE′	$R^2 = 0.992$	$F(1,40) = 5015.0$	$P < 0.001$
Xiuhe	SL′ = 0.0044RE′	$R^2 = 0.987$	$F(1,45) = 3382.2$	$P < 0.001$

SL′ cumulative sediment load, *RE′* cumulative rainfall erosivity

Table 6 The effects of rainfall erosivity and human intervention on annual sediment load change in the PYLB

Basin	Period	Rainfall erosivity (MJ mm ha^{-1} h^{-1} year^{-1})	Predicted sediment load (10^4 t year^{-1})	Observed sediment load (10^4 t year^{-1})	Impact of rainfall erosivity variability		Impact of human activities	
					Amount (10^4 t year^{-1})	Percentage (%)	Amount (10^4 t year^{-1})	Percentage (%)
The entire	1961–1984	9580.5	1677.5	1690.4				
PYLB	1985–2002	10,414.8	1823.6	1053.8	146.1	8.0	− 915.9	− 50.2
	2003–2014	9789.2	1714.1	556.0	36.5	2.1	− 1194.6	− 69.7
Ganjiang	1961–1984	8544.3	1203.9	1200.5				
	1985–1998	8724.1	1229.2	694.5	25.3	2.1	− 560.1	− 45.6
	1999–2014	8917.4	1256.5	299.7	52.6	4.2	− 1009.3	− 80.3
Fuhe	1961–2002	10,550.8	151.9	149.3				
	2003–2014	10,121.2	145.7	96.2	− 6.2	− 4.2	− 43.4	− 29.8
Xinjiang	1961–2000	11,262.8	252.3	233.2				
	2001–2014	11,207.3	251.0	100.7	− 1.2	− 0.5	− 149.1	− 59.4
Xiuhe	1961–2000	9610.9	42.3	39.4				
	2001–2014	8958.5	39.4	16.9	− 2.9	− 7.3	− 19.7	− 49.9

5 Discussions

Modeling soil erosion is complicated because soil loss varies spatially and temporally depending on many factors, such as the rainfall, soil characteristics, geographic and geomorphic conditions, and their interactions (De Santos Loureiroa and De Azevedo Coutinho 1995). Soil loss is proportional to the rainfall erosivity factor (R) when other factors are held constant. Compared with other regions in China, rainfall erosivity in the PYLB was much higher than the Loess Plateau (1301.5 MJ mm ha^{-1} h^{-1} year^{-1}) (Xin et al. 2011), while was much lower than Guangdong province (13,758.0 MJ mm ha^{-1} h^{-1} year^{-1}) (Luo et al. 2010). These inconsistent results may be explained by the different climate zones of the study area. The Loess Plateau belongs to the continental monsoon region, where the average annual precipitation was about 450 mm year^{-1} (Xin et al. 2011). The Guangdong province is characterized by oceanic monsoon climate, in which the annual precipitation was often more than 1500 mm year^{-1} (Luo et al. 2010). Additionally, precipitation in Guangdong is affected greatly by the frequent convective typhoon rainfall events, which may lead to high rainfall erosivity (Luo et al. 2010). With the same climate system, rainfall erosivity of the PYLB is similar to the Pearl River basin (9918.9 MJ mm ha^{-1} h^{-1} year^{-1}) (Lai et al. 2016).

Annual rainfall erosivity of the PYLB showed insignificant temporal trend, which is consistent with most other districts in China (Luo et al. 2010; Huang et al. 2013; Lai et al. 2016). However, rainfall erosivity in winter, January, and August was in a significant increasing trend (Table 2). The results indicated soil erosion risk of the PYLB in these periods was great. The inter- and intra-annual change of rainfall erosivity and annual rainfall demonstrated that variation of rainfall erosivity is more intensive than annual rainfall (Fig. 3). We established the linear relationship between the anomaly percentage of rainfall erosivity and the anomaly percentage of annual rainfall. The equation can be expressed as $y = 1.598x$ ($R^2 = 0.807$, $n = 54$), which implied that the rainfall erosivity changed by 1.598% when the annual rainfall change was 1%. It revealed that a small change in annual rainfall would lead to a big variation in rainfall erosivity, indicating the necessity of investigating rainfall erosivity to estimate the risk of regional soil erosive. This is primarily because rainfall erosivity is closely related to rainfall intensity (Angulo-Martínez and Beguería 2009). The magnitude of change in rainfall erosivity was higher than that of annual rainfall as the result of the rainfall change is often accompanied with rainfall intensity variability (Xin et al. 2011). Zhang et al. (2005) found that the percentage changes in rainfall erosivity were about 1.2–1.4-fold greater than percentage changes in total precipitation in the Yellow River basin. De Santos Loureiroa and De Azevedo Coutinho (1995) found that the annual rainfall erosivity increased (17%) greater than annual

Table 7 The transition matrix of land use and cover in PYLB from 1980 to 2000 (km^2)

2000 1985	Arable land	Forestland	Grassland	Water	Built-up land	Barren land	Total in 1985
Arable land	44508.87	265.30	19.08	206.28	504.64	0.06	45504.23
Forestland	289.38	102941.30	136.27	31.11	125.04	1.19	103524.29
Grassland	64.88	519.20	6932.23	17.92	11.88	0.03	7546.14
Water	250.66	12.30	18.93	6457.12	25.44	0	6764.45
Built-up land	16.90	1.94	0.41	13.06	2653.70	0	2686.01
Barren land	0.58	0.76	0	302.26	0.16	630.63	934.34
Total in 2000	45131.27	103740.80	7106.92	7027.75	3320.86	631.91	166959.51

Notes: the data was cited from Fan et al. (2009).

rainfall change (9%) in the Southern Portugal. They were all consistent with this paper. Rainfall erosivity was more relevant to sediment load before change-point for the cause of rainfall erosivity reflects both the information of the rainfall amount and rainfall intensity (Table 4). Hence, it is more reasonable to select rainfall erosivity as the independent variable of the double mass curves than annual rainfall and erosive rainfall."

Our study illustrated rainfall erosivity change was not the dominant factor of the sediment load reduction in the PYLB (Table 6), which means the reduction of sediment load in the PYLB mainly attributed to anthropogenic activities. Before 1980s, soil erosion in the PYLB has not been effectively governed due to the "Cultural Revolution" (1966–1976, a period which witnessed a great amount of rapid deforestation) (Zhang et al. 2011a, b). Serious soil erosion caused high sediment load in the five tributaries. In the 1980s, with the beginning of the "Chinese Economic Reform and Opening-up" and the rapid development of the national economy, soil and water conservation work in the PYLB has also received strong economic support from the government. As a result, forest coverage in the PYLB increased significantly since 1980s (Min et al. 2011). Forest coverage of the basin was only about 30% in the 1970s, while it recovered to over 60% at the end of the 1990s owing to large-scale implementation of soil and water conservation measures (Gu et al. 2016a, b). Undoubtedly, higher forest coverage would reduce the sediment load because the amount of rainfall transformed into runoff was lessened (Gao et al. 2011). The change-points of the Ganjiang River and the entire PYLB in 1985 may confirm the great influences of forest cover on sediment load (Fig. 6). The Ganjiang basin selected as a demonstration site of soil and water conservation work in the PYLB, which carried out the soil and water conservation management as early as 1984 (Gu et al. 2016a, b). Consequently, the change-point in 1985 of sediment load in the Ganjiang River was earlier than other tributaries. Sediment load of Ganjiang River accounts for more than 60% of the total amount of the five tributaries (Zhang et al. 2011a, b), thus total sediment load inputs of the PYL emerged downward shift in 1985. Besides, land use and land cover change (LUCC) also affect basin sediment yield (Gao et al. 2011; Walling (2006). Fan et al. (2009) investigated the LUCC in PYLB in 1985 and 2000 (Table 7). Results showed that arable land, grassland, and barren land decreased 372.96 km^2 (0.82%), 439.22 km^2 (5.82%), and 302.43 km^2 (32.37%), while forestland, water, and built-up land increased 216.51 km^2 (0.21%), 263.30 km^2 (3.89%), and 634.85 km^2 (23.64%) from 1985 to 2000 (Table 7). The transition in land use inevitably caused sediment load change in the basin. However, the specific changes of sediment load due to LUCC were unavailable in the study because of data limitation.

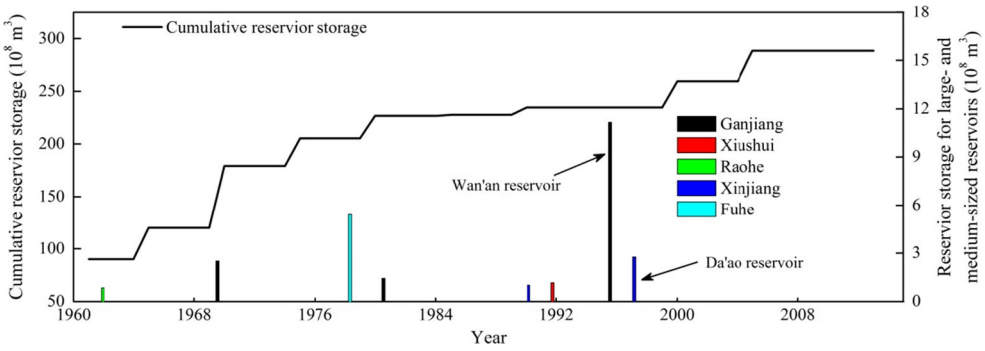

Fig. 10 Cumulative reservoir storage and the large- and medium-sized reservoirs in the PYLB (the bar charts donate large- and medium-sized reservoirs along the five tributaries)

Previous studies have found that construction of the reservoir have a great effects on the reduction of river sediment load (Walling 2006; Mu et al. 2012; Luo et al. 2015). Figure 10 shows that cumulative reservoir storage increased evidently from 1961 to 2013 in the PYLB, which could store a large amount of the sediment load caused by rainfall erosvity, leading to reduction of sediment load inputs of the PYL. There was a significant negative correlation ($r = -0.489$, $P < 0.01$) between annual sediment load of the entire PYLB and cumulative reservoir storage across the PYLB. Moreover, other change-points of the sediment load (i.e., 2003, 1999, and 2001) were closely related to the construction of large- and medium-sized reservoir in the PYLB. The largest reservoir in the Ganjiang River, Wan'an Reservoir (storage capacity 11.16×10^8 m^3), was established in 1996, which can retain 2336×10^3 t of sediment load per year (Fig. 10) (Guo et al. 2006). It resulted in enormous decrease in sediment load, causing sediment load in Ganjiang River appeared downward shift in 1999 (Fig. 6) (Zhang et al. 2011a, b). Da'ao Reservoir in the Xinjiang River with a storage capacity of 2.76×10^8 m^3 was built in 1997, which intercept large amount of sediment from the upstream of the dam (Fig. 10). This was the main reason for the abrupt change in sediment load of Xinjiang River in 2001. Ganjiang and Xinjiang rivers were the two largest tributaries of the Poyang Lake basin. Therefore, total sediment load inputs of the PYL emerged abrupt change in 2003, which was followed by the shift time of the above two tributaries. The total storage capacity of reservoir in Ganjiang River was larger than other tributaries, thereby the effects of human activities on sediment load decline was the highest (80.3%) among the tributaries (Table 6). There was no change-point of sediment load in the Raohe River, which has the least reservoirs in the river basin (Fig. 10). This study focused on the impacts of vegetation recovery and reservoir construction on sediment load, while other human activities, such as sand mining and river regulation, were not taken into account.

he above analysis suggests that soil and water loss situation in the PYLB is optimistic. However, causes of soil erosion in the PYLB became complicated after 2000. Luo et al. (2015) found that area of intensive erosion (> 5000 t km^{-2} year^{-1}) in the PYLB increased after 2000 even though the total soil erosion area showed a decreasing trend from the 1980s to the 2000s. Moreover, collapsing erosion (a special type of soil erosion occurred in hilly red soil areas of southern China) in the upper reaches of Ganjiang basin is still severe, and there is no effective measure to completely manage it so far (Liang et al. 2009). Rainfall erosivity for most stations showed upward trend, especially, rainfall erosivity increased significantly in winter (Fig. 5e), which may aggravate the soil erosion in the PYLB. Besides, our results revealed that the periodic oscillation of sediment load was in accordance with rainfall erosivity, and their main periods unchanged over the past 54 years (Fig. 8). Consequently, it is still essential to take effective conservation measures to safeguard water and soil resources in the PYLB.

6 Conclusions

In this study, the spatiotemporal variation of rainfall erosivity in the Poyang Lake basin (PYLB) of China during 1961–2014 was investigated based on Zhang's model. Results showed that average annual rainfall erosivity in the PYLB was 9905.0 MJ mm ha^{-1} h^{-1} year^{-1} over the last 54 years. No significant temporal trend was detected in annual rainfall erosivity, while significant increasing trend was detected in rainfall erosivity in winter. For monthly rainfall erosivity, significant increasing trend was found in 57.9% of the stations in January, which was deemed as the main reason for rainfall erosivity significantly increased in winter. In such context, annual sediment load inputs of the PYLB showed a significant decreasing trend with change-points in 1985 and 2003, over the same period. Compared with the period of 1961–1984, average annual sediment load has decreased by 44.4 and 72.1% during 1985–2002 and 2003–2014, respectively. Relationships of sediment load and rainfall erosivity were significantly changed after change-points, but the periodicity of sediment load and rainfall erosivity unchanged in the last half century. It was found that the non-rainfall erosivity factors (human activity) were the dominant cause for sediment load decline. Soil and water conservation, construction of reservoir have played a more prominent role in sediment load reduction in the PYLB.

Acknowledgments This work was supported by Special-Funds of Scientific Research Programs of State Key Laboratory of Soil Erosion and Dryland Farming on the Loess Plateau (A314021403-Q2), the Non-profit Industry Financial Program of MWR, China (201501049), Science & Technology Development Foundation of Northwest A&F University (A289021104), and Youth Innovation Promotion Association, Chinese Academy of Sciences (2011289).

References

Angulo-Martínez M, Beguería S (2009) Estimating rainfall erosivity from daily precipitation records: a comparison among methods using data from the Ebro Basin (NE Spain). J Hydrol 379(1):111–121

Bonilla CA, Vidal KL (2011) Rainfall erosivity in central Chile. J Hydrol 410(1):126–133

Chow GC (1960) Tests of equality between sets of coefficients in two linear regressions. Econometrica:591–605

De Santos Loureiroa N, De Azevedo Coutinho M (1995) Rainfall changes and rainfall erosivity increase in the Algarve (Portugal). Catena 24(1):55–67

Fan ZW, Huang LG, Qian HY, Fang Y (2009) Soil erosion effects driven by land use changes over the Poyang Lake Basin (in Chinese). Resour Sci 31(10):1787–1792

Flanagan D, Nearing M (1995) USDA-Water Erosion Prediction Project: hillslope profile and watershed model documentation. NSERL report

Gao P, Mu X-M, Wang F, Li R (2011) Changes in streamflow and sediment discharge and the response to human activities in the middle reaches of the Yellow River. Hydrol Earth Syst Sci 15(1):1–10

Gu C, Mu X, Gao P, Wang X (2016a) Variation of runoff and sediment discharge and response to human activities in the Ganjiang River (in Chinese). J Sediment Res (03): 38-44

Gu C, Mu X, Zhao G, Gao P, Sun W, Yu Q (2016b) Changes in stream flow and their relationships with climatic variations and anthropogenic activities in the Poyang Lake Basin, China. Water 8(12):564

Guo H, Jiang T, Wang G, Su B, Wang Y (2006) Observed trends and jumps of climate change over Lake Poyang Basin, China: 1961-2003 (in Chinese). J Lake Sci 18(5):443–451

He B, Miao C, Shi W (2013) Trend, abrupt change, and periodicity of streamflow in the mainstream of Yellow River. Environ Monit Assess 185(7):6187–6199

Huang J, Zhang J, Zhang Z, Xu C-Y (2013) Spatial and temporal variations in rainfall erosivity during 1960–2005 in the Yangtze River basin. Stoch Env Res Risk A 27(2):337–351

Kendall MG (1975) Rank correlation methods

Lai C, Chen X, Wang Z, Wu X, Zhao S, Wu X, Bai W (2016) Spatio-temporal variation in rainfall erosivity during 1960–2012 in the Pearl River Basin, China. Catena 137:382–391

Lal R (2003) Soil erosion and the global carbon budget. Environ Int 29(4):437–450

Liang Y, Ning D, Pang X, Li D, Zhang B (2009) TThe characteristics and governance of collapsing erosion in the southern red soil erosion area in China. Soil and water conservation in china 29(01):31-34 (in Chinese)

Luo J, RONG Y, Chen L, Dai L, Hu Y (2010) Long-term trend of rainfall erosivity in Guangdong Province from 1960 to 2007 (in Chinese). J China Hydrol 30(1):79–83

Luo W, Zhang X, Deng Z, Chen L, Chris G (2015) Runoff and sediment load transport and cause analysis in Poyang Lake basin over the period 1956-2008 (in Chinese). Adv Water Sci 2014(05):658–667

Ma L, Jiang G, Zuo C, Qiu G, Huo H (2009) Spatial and temporal distribution characteristics of rainfall erosivity changes in Jiangxi province over more than 50 years (in Chinese). Trans Chin Soc Agric Eng 25(10):61–68

Mann HB (1945) Nonparametric tests against trend. Econometrica:245–259

Meusburger K, Steel A, Panagos P, Montanarella L, Alewell C (2012) Spatial and temporal variability of rainfall erosivity factor for Switzerland. Hydrol Earth Syst Sci 16(1):167–177

Min Q, Shi J, Min D (2011) Characteristics of sediment into and out of Poyanghu Lake from 1956 to 2005 (in Chinese). J China Hydrol 31(01):54–58

Morgan R, Quinton J, Smith R, Govers G, Poesen J, Auerswald K, Chisci G, Torri D, Styczen M (1998) The European Soil Erosion Model (EUROSEM): a dynamic approach for predicting sediment transport from fields and small catchments. Earth Surf Process Landf 23(6): 527–544

Mu X, Zhang X, Shao H, Gao P, Wang F, Jiao J, Zhu J (2012) Dynamic changes of sediment discharge and the influencing factors in the Yellow River, China, for the recent 90 years. Clean Soil Air Water 40(3):303–309

Oduro-Afriyie K (1996) Rainfall erosivity map for Ghana. Geoderma 74(1):161–166

Onori F, De Bonis P, Grauso S (2006) Soil erosion prediction at the basin scale using the revised universal soil loss equation (RUSLE) in a catchment of Sicily (southern Italy). Environ Geol 50(8):1129–1140

Qin W, Zuo C, Zheng H, Ma L, Du P (2013) Determination of key factors of soil loss equation of red-soil slop land in northern Jiangxi province (in Chinese). Trans Chin Soc Agric Eng 29(21):115–125

Renard KG, Freimund JR (1994) Using monthly precipitation data to estimate the R-factor in the revised USLE. J Hydrol 157(1):287–306

Renard K, Foster G, Weesies G, McCool D, Yoder D (1997) RUSLE a guide to conservation planning with the revised universal soil loss equation. USDA Agricultural Handbook 703

Renschler C, Mannaerts C, Diekkrüger B (1999) Evaluating spatial and temporal variability in soil erosion risk—rainfall erosivity and soil loss ratios in Andalusia, Spain. Catena 34(3):209–225

Rodionov SN (2006) Use of prewhitening in climate regime shift detection. Geophys Res Lett 33(12)

Romero LD, Muñoz JLA, Marín APG (2007) Annual distribution of rainfall erosivity in western Andalusia, southern Spain. J Soil Water Conserv 62(6):390–403

Scherr SJ, Yadav S (1996) Land degradation in the developing world: Implications for food, agriculture, and the environment to 2020

Shi Z, Cai C, Ding S, Wang T, Chow T (2004) Soil conservation planning at the small watershed level using RUSLE with GIS: a case study in the Three Gorge Area of China. Catena 55(1):33–48

Shi Z, Zhang T, Gao H (2008) Water and soil loss characteristics in Poyanghu Lake Basin (in Chinese). J Yangtze River Sci Res Inst 25:38–41

Sun S, Chen H, Ju W, Song J, Zhang H, Sun J, Fang Y (2013) Effects of climate change on annual streamflow using climate elasticity in Poyang Lake Basin, China. Theor Appl Climatol 112(1–2):169–183

Sun W, Mu X, Song X, Wu D, Cheng A, Qiu B (2016) Changes in extreme temperature and precipitation events in the Loess Plateau (China) during 1960–2013 under global warming. Atmos Res 168: 33–48

Torrence C, Compo GP (1998) A practical guide to wavelet analysis. Bull Am Meteorol Soc 79(1):61–78

Van der Knijff J, Jones R, Montanarella L (2000) Soil erosion risk assessment in Europe. European Soil Bureau, European Commission Belgium

Von Storch H (1999) Misuses of statistical analysis in climate research. In: Analysis of climate variability. Springer, Berlin, pp 11–26

Walling D (2006) Human impact on land–ocean sediment transfer by the world's rivers. Geomorphology 79(3):192–216

Wischmeier WH, Smith DD (1958) Rainfall energy and its relationship to soil loss. EOS Trans Am Geophys Union 39(2):285–291

Wischmeier WH, Smith DD (1978) Predicting rainfall erosion losses. A Guide to Conservation Planning. US Department of Agriculture, Agricultural Handbook, Washington, DC, p 537

Xiaoli Z, Zengxiang Z, Quanbin Z (2002) Soil erosion actuality and its synthesis prevention countermeasures in China (in Chinese). J Soil Water Conserv 16(1):40–43

Xin Z, Yu X, Li Q, Lu X (2011) Spatiotemporal variation in rainfall erosivity on the Chinese Loess Plateau during the period 1956–2008. Reg Environ Chang 11(1):149–159

Xu Y, Xu C, Gao X, Luo Y (2009) Projected changes in temperature and precipitation extremes over the Yangtze River Basin of China in the 21st century. Quat Int 208(1):44–52

Yu B, Rosewell C (1996) An assessment of a daily rainfall erosivity model for New South Wales. Soil Res 34(1):139–152

Yue S, Wang C (2004) The Mann-Kendall test modified by effective sample size to detect trend in serially correlated hydrological series. Water Resour Manag 18(3):201–218

Zhang W-B, Xie Y, Liu B-Y (2002) Rainfall erosivity estimation using daily rainfall amounts (in Chinese). Sci Geogr Sin 22(6):705–711

Zhang G-H, Nearing M, Liu B-Y (2005) Potential effects of climate change on rainfall erosivity in the Yellow River basin of China. Trans ASAE 48(2):511–517

Zhang Q, Sun P, Chen X, Jiang T (2011a) Hydrological extremes in the Poyang Lake basin, China: changing properties, causes and impacts. Hydrol Process 25(20):3121–3130

Zhang Q, Sun P, Jiang T, Tu X, Chen X (2011b) Spatio-temporal patterns of hydrological processes and their responses to human activities in the Poyang Lake basin, China. Hydrol Sci J 56(2):305–318

Zhang Q, Liu J, Singh VP, Gu X, Chen X (2016a) Evaluation of impacts of climate change and human activities on streamflow in the Poyang Lake basin, China. Hydrol Process 30:2562–2576

Zhang Q, Xiao M, Singh VP, Wang Y (2016b) Spatiotemporal variations of temperature and precipitation extremes in the Poyang Lake basin, China. Theor Appl Climatol 124(3–4):855–864

Zhao G, Mu X, Jiao J, An Z, Klik A, Wang F, Jiao F, Yue X, Gao P, Sun W (2017) Evidence and causes of spatiotemporal changes in runoff and sediment yield on the Chinese loess plateau. Land Degrad Dev 28(2):579–590